ELSEVIER

Speciation of precious metal anti-cancer complexes by NMR spectroscopy

Taotao Zou[1,2], Peter J. Sadler[1,*]

[1]Department of Chemistry, University of Warwick, Gibbet Hill Road, Coventry CV4 7AL, UK
[2]State Key Laboratory of Synthetic Chemistry, Department of Chemistry, The University of Hong Kong, Pokfulam Road, Hong Kong, China

CrossMark

Understanding the mechanism of action of anti-cancer agents is of paramount importance for drug development. NMR spectroscopy can provide insights into the kinetics and thermodynamics of the binding of metallodrugs to biomolecules. NMR is most sensitive for highly abundant $I = 1/2$ nuclei with large magnetic moments. Polarization transfer can enhance NMR signals of insensitive nuclei at physiologically-relevant concentrations. This paper reviews NMR methods for speciation of precious metal anti-cancer complexes, including platinum-group and gold-based anti-cancer agents. Examples of NMR studies involving interactions with DNA and proteins in particular are highlighted.

Section editor:
Francois M.U. Dufrasne, Université Libre de Bruxelles, Brussels, Belgium.

Introduction

The successful clinical application of cisplatin and its second (carboplatin) and third (oxaliplatin) generation derivatives to treat cancers has greatly stimulated interest in metal-based anti-cancer agents. Many precious metal (Ru, Rh, Os, Ir, Pt and Au) coordination complexes are now showing promising anti-tumor activity [1,2]. Understanding the thermodynamic stability of metal complexes and the kinetics of their reactions with biomolecules is crucial for elucidating their mechanisms of action. Both the ligand and metal ion can play important roles in the anti-cancer effects. Nuclear magnetic

resonance (NMR) spectroscopy, the absorption of electromagnetic radiation by magnetic nuclei, is a powerful method for speciation of metal complexes in solution and in biological systems. NMR spectroscopy can often be used to determine not only the structures of molecules (ca. <30 kDa) in solution, but also the strength of metal binding to biomolecules (equilibrium constants, including DNA and proteins) and kinetics of dynamic processes (including rates of ligand exchange on a microsecond to second timescale). This review summarizes the application of NMR methods to speciation in biological systems, with a focus on platinum-group and gold-based anti-cancer complexes in solution.

NMR sensitivity

In principle, NMR signals can be detected for all isotopes that have non-zero nuclear spins (i.e., an odd number of neutrons or protons in their nuclei). The spin (I)-1/2 nuclei (e.g., ^{1}H, ^{13}C, ^{15}N, ^{19}F, ^{31}P, ^{195}Pt) are the most widely studied. The $I > 1/2$ nuclei (quadruplar nuclei) are less useful in practical NMR applications due to their broad NMR signals caused by rapid quadrupolar relaxation, with the exception of symmetrical environments [3]. Unfortunately, ~75% stable magnetic nuclides have $I > 1/2$. For platinum-group and gold metals, nuclei of interest are ^{195}Pt (natural abundance

Corresponding author: P.J. Sadler (P.J.Sadler@warwick.ac.uk)

Table 1. NMR responsive ligand nuclei and metal ion nuclei.

Isotope	Abundance (%)	Nuclear spin (I)	Magnetogyric ratio (γ, $\times 10^7$ rad/Ts)	Relative sensitivity (^{1}H = 1.00)	Quadruple moment (10^{28}*Q/m^2)	Chemical shift range (ppm)
^{1}H	99.98	1/2	26.7519	1.00	0	+20 to −50
^{2}H	1.5×10^{-2}	1	4.1066	9.65×10^{-6}	0.0028	+12 to −25
^{3}H	0	1/2	28.535	1.21	0	+12 to −25
^{6}Li	7.42	1	3.9371	8.5×10^{-3}	−0.0008	+3 to −9
^{7}Li	92.58	3/2	10.3976	0.29	−0.04	+3 to −10
^{10}B	19.58	3	2.875	1.99×10^{-2}	8.5×10^{-2}	+100 to −100
^{11}B	80.42	3/2	8.584	0.17	4.1×10^{-2}	+100 to −120
^{13}C	1.108	1/2	6.7283	1.59×10^{-2}	0	+250 to −25
^{14}N	99.635	1	1.9338	1.01×10^{-3}	0.0199	+800 to −400
^{15}N	0.365	1/2	−2.712	1.04×10^{-3}	0	+620 to −420
^{17}O	3.7×10^{-2}	5/2	−3.6279	3.7×10^{-2}	−3.6279	+1600 to −50
^{19}F	100	1/2	25.181	0.83	0	+900 to −500
^{23}Na	100	3/2	7.0801	9.25×10^{-2}	0.1	+20 to −70
^{29}Si	4.7	1/2	−5.3188	7.84×10^{-3}	0	+270 to −580
^{31}P	100	1/2	10.841	6.63×10^{-2}	0	+1400 to −500
^{33}S	0.76	3/2	2.055	2.26×10^{-3}	−0.055	+400 to −600
^{35}Cl	75.53	3/2	2.624	4.7×10^{-3}	−0.1	+1000 to −200
^{37}Cl	24.47	3/2	2.1842	2.71×10^{-3}	−0.079	+1000 to −200
^{79}Br	50.54	3/2	6.7228	7.86×10^{-2}	0.37	–
^{81}Br	49.46	3/2	7.2468	9.85×10^{-2}	0.31	–
^{99}Ru	12.72	3/2	−1.234	1.95×10^{-4}	0.076	+8000 to −1000
^{100}Ru	17.07	5/2	−1.383	1.41×10^{-3}	0.44	–
^{103}Rh	100	1/2	−0.846	3.11×10^{-5}	0	+10 000 to −2000
^{105}Pd	22.2	5/2	−1.2305		0.65	+8000 to −1000
^{127}I	100	5/2	5.3817	9.34×10^{-2}	−0.79	–
^{187}Os	1.64	1/2	0.616	1.22×10^{-5}	0	–
^{189}Os	16.1	3/2	0.8475	2.34×10^{-3}	0.8	–
^{191}Ir	37.3	3/2	0.4643	2.53×10^{-5}	1.1	–
^{193}Ir	62.7	3/2	0.5054	3.27×10^{-5}	1.0	–
^{195}Pt	33.7	1/2	5.768	9.94×10^{-3}	0	+11 840 to −3000
^{197}Au	100	3/2	0.4625	2.51×10^{-5}	0.59	–

Source: http://www.bruker-nmr.de/guide/eNMR/chem/NMRnuclei.html; http://www-usr.rider.edu/~grushow/nmr/NMR_tutor/periodic_table/.

of 33.7%), ^{187}Os (1.64%) and ^{103}Rh (100%) with $I = 1/2$, but their sensitivity is not high (especially ^{187}Os and ^{103}Rh). NMR signal intensity is proportional to $B_0^2\gamma^3$ (B_0 is magnetic field, γ is magnetogyric ratio), while the signal-to-noise ratio is proportional to $B_0^{3/2}\gamma^{5/2}$. Taking ^{195}Pt as an example, $\gamma(^{195}$Pt) is ~4.6-fold lower than $\gamma(^1$H), and hence the relative intensity of ^{195}Pt is ~100 times lower than that of ^{1}H. ^{187}Os and ^{103}Rh nuclei are even less sensitive due to much lower magnetogyric ratios. Table 1 lists some NMR parameters of ligand and metal nuclei of interest for NMR studies in biological systems.

Polarization transfer methods, such as DEPT (Distortionless Enhancement by Polarization Transfer), can enhance NMR sensitivity for low magnetogyric ratio nuclei [4,5]. INEPT (Insensitive Nuclei Enhanced by Polarization Transfer) can enhance signal intensities by transferring nuclear spin polarization from sensitive spins (I, usually ^{1}H) to the less sensitive nucleus (S) [5]. The sensitivity can be increased by a factor of γ(I)/γ(S) through INEPT. Heteronuclear Single-Quantum Correlation spectroscopy (HSQC) utilizes INEPT to transfer the magnetization from ^{1}H to a nearby heteronucleus linked through one bond, resulting in 2D NMR spectra (e.g.

[^{1}H,^{13}C] HSQC, [^{1}H,^{15}N] HSQC). Heteronuclear Multiple-Quantum Correlation spectra (HMQC) are almost identical to HSQC spectra. However, there are few metal complexes in which ^{1}H is directly bound to a metal. In other cases, Heteronuclear Multiple-Bond Correlation spectroscopy (HMBC) can be helpful, since it is possible to detect nuclei coupled to more distant protons. HMBC utilizes long-range coupling to ^{1}H nuclei, usually through 2–4 bonds.

NMR studies of precious metal complexes in biological systems

The speciation of metal complexes can be investigated by NMR through either ligand nuclei or metal nuclei. Among the platinum group and gold nuclei, only ^{195}Pt has a reasonable sensitivity for NMR (relative sensitivity compared to ^{1}H 9.94×10^{-3}). Therefore, the speciation of these metal complexes is mostly focused on ligand nuclei. Another issue is the paramagnetic effect, which leads to shifts and broadening of NMR signals. Thus, the oxidation state of the metal should be considered if sharp NMR signals are anticipated.

Ruthenium

Ru(III) (low-spin 4d^5) complexes, such as the anti-metastatic drug NAMI-A (H$_2$Im[$trans$-RuCl$_4$(DMSO)HIm], HIm = 1H-imidazole) and anti-cancer KP1019 [H$_2$ind][$trans$-RuCl$_4$(Hind)$_2$] (Hind = 1H-indazole), are paramagnetic; however, their paramagnetic NMR spectra are still obtainable and useful for studying their transformation in biological environments. The ^{1}H NMR spectrum of $trans$-[RuCl$_4$(Him)$_2$]$^-$ in D$_2$O (Fig. 1A) in D$_2$O shows three broad peaks (δ = −5.87, −15.83 and −21.25 ppm) assignable to coordinated imidazole [6]. A stepwise exchange of Cl by D$_2$O is observed over a period of 16.6 hours at 310 K. Ru(III) polycarboxylates have been used to treat septic shock caused by bacteria-induced NO formation. These complexes react readily with NO to form [RuNO] species with reduction of Ru^{III} to Ru^{II} and oxidation of NO to NO$^+$, forming stable Ru–NO bonds. Reaction of [Ru^{II}(hedta)]$^-$ (hedta^{3-} = N-(hydroxyethyl)ethylenediaminetriacetate) with NO gives an ^{15}N NMR peak for [Ru^{II}(hedta)(^{15}NO$^+$)] δ(^{15}N) at 249.6 ppm (Fig. 1B), while the two-electron reduction product [Ru^{II}(hedta)(^{15}NO$^-$)]$^{2-}$ is a mixture of cis- and $trans$-equatorial isomers, δ(^{15}N) at 609.4 and 607.4 ppm [7].

NMR can distinguish stereoisomers of octahedral Ru(II) complexes. Xie et $al.$ have combined double quantum-filtered correlation spectroscopy (DQF-COSY), HSQC, HMBC and NOESY experiments to study the stereochemistry of Ru(II) polypyridyl complexes (Fig. 1C) and fully assigned the NMR signals of enantiomers [8]. A unique binding mode between the anticancer complex [(η^6-biphenyl)Ru(en)Cl]$^+$ and DNA with Ru(II) coordinated to N7 of guanine and concomitant π-stacking intercalation of the non-coordinated phenyl group into nearby base pairs has been characterized by NMR (Table 2, entries 1 and 2) [9]. The analogous complex, [(η^6-tha) Ru(en)Cl]$^+$ (tha = tetrahydroanthracene), also exhibits combined coordinative bonding and intercalation [10].

Rhodium

^{103}Rh is highly abundant (100%) with I = 1/2, but has a very low magnetogyric ratio (Table 1). The ^{103}Rh NMR chemical shifts of [(COD)Rh^I(Phosphine)X] complexes, recorded using inverse 2D [^{1}H,^{103}Rh] and [^{31}P,^{103}Rh]{^{1}H} NMR, range from +557 to −332 ppm [11]. Dirhodium(II) acetate complexes are spin-paired and diamagnetic. 2D NMR studies by Dunbar et $al.$ revealed an intrastrand binding between cis-[Rh$_2$(μ-O$_2$CCH$_3$)$_2$(η^1-O$_2$CCH$_3$)]$^+$ and DNA (Table 2, entry 3) [12]. The binding of the two Rh centers to C5 and A6 results in significant disruption of H-bonds between base pairs and hence destabilizes the DNA duplex. They also reported an interesting binding mode of cis-[Rh$_2$(dap)(μ-O$_2$CCH$_3$)$_2$(η^1-O$_2$CCH$_3$)(CH$_3$OH)](O$_2$CCH$_3$)]$^+$ (dap = 1,12-diazaperylene) binding with a DNA oligonucleotide (Table 2, entry 4) [13]. NMR studies indicated binding between one Rh and N7 of adenine and a cooperative intercalative binding via the dap ligand (on the other Rh center) stacking with the same adenine. The octahedral rhodium(III) complexes developed by Barton and coworkers can specifically recognize mismatched DNA. The binding interactions of the Δ-[Rh(bpy)$_2$chrysi]$^{3+}$ (chrysi = 5,6-chrysenequinonediimine) with CC mismatched DNA oligomers have been studied by NMR (Table 2, entry 5) [14]. NOESY and COSY experiments indicate a deep insertion into a minor grove site of CC mismatched DNA and such binding does not significantly alter the conformation of DNA.

Osmium

^{187}Os also has I = 1/2, but NMR observation is hampered by its low natural abundance (1.61%) and small magnetogyric ratio. Bell et $al.$ have studied [Os(arene)X$_2$L] complexes using inverse [^{1}H,^{187}Os] and [^{31}P,^{187}Os]{^{1}H} NMR. There is a large δ(^{187}Os) range from −1697 to −5265 ppm [15]. Meanwhile, the effects of ligand electronic properties and steric effects on δ(^{187}Os) have been separately compared by variation of arene, halide and phosphine ligands. Gray et $al.$ have reported the [^{1}H,^{187}Os] HMBC spectrum of [Os(η^6-biphenyl)$_2$](OTf)$_2$ complex (Fig. 1D) [16]. Interestingly, coupling between all the protons and ^{187}Os was detected, except for H^8 which is the furthest away. Fu et $al.$ studied hydrolysis and DNA binding of anti-cancer Os^{II} complexes [Os(η^6-arene)(XY)Z]PF$_6$ (arene = p-cymene, XY = Impy-NMe$_2$, and Z = Cl) by ^{1}H NMR [17]. The Os^{II} complex undergoes hydrolysis to 99% extent after incubation at 310 K for 24 hours. The aqua adduct can bind to 9-EtG, as revealed by the downfield shift of ^{1}H resonances of the Os^{II} ligand and upfield shift of 9-EtG H8. More importantly, the aqua adduct can oxidize NADH to NAD$^+$ catalytically via forming a hydride adduct with a ^{1}H signal at −4.2 ppm.
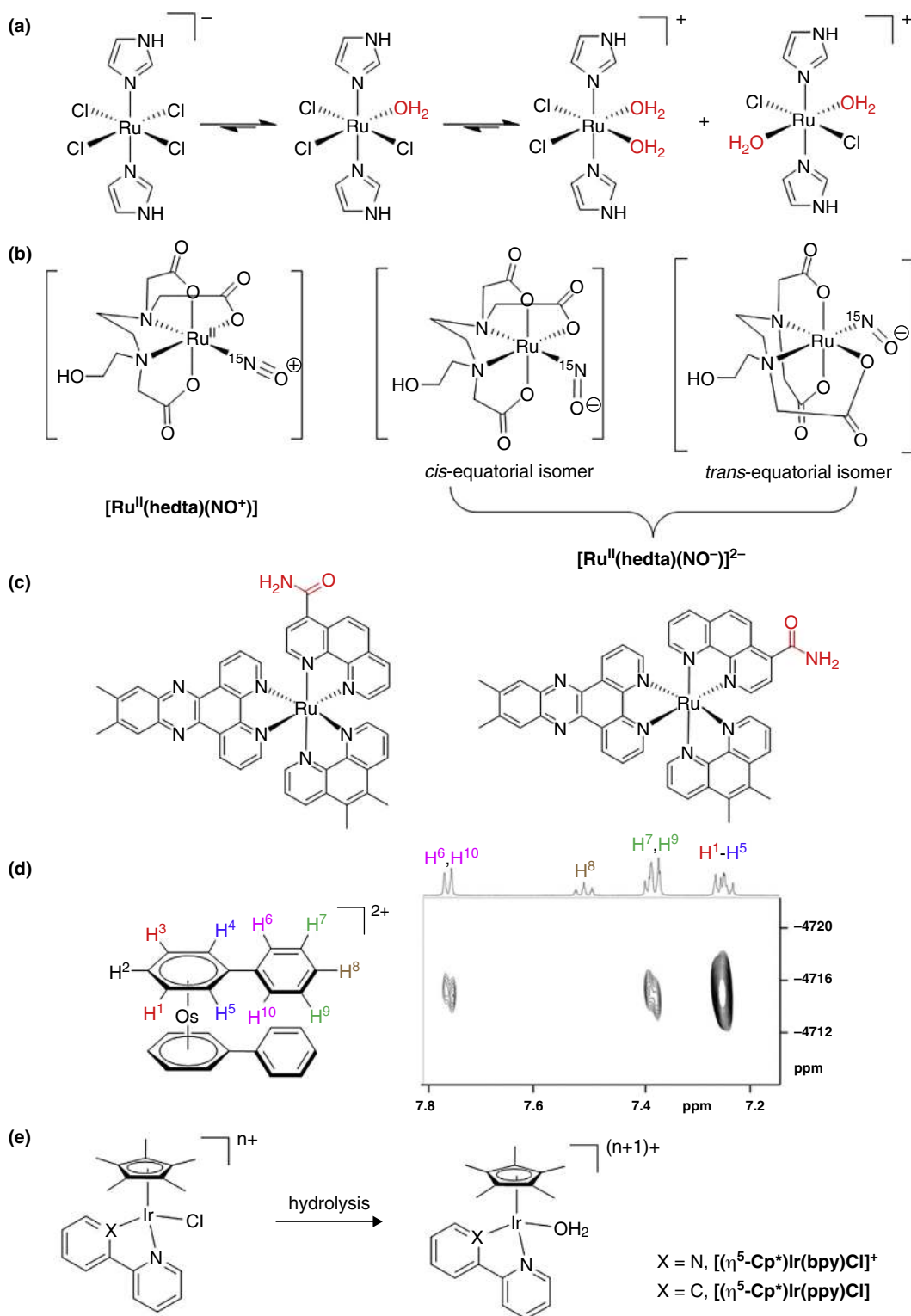
Figure 1. (a) Stepwise hydrolysis of *trans*-[RuCl$_4$(Him)$_2$]$^-$, a Ru(III) complex closely related to KP1019. (b) Structures of [Ru^{II}(hedta)(^{15}NO$^+$)] and [Ru^{II}(hedta)(^{15}NO$^-$)]$^{2-}$. (c) Stereoisomers of Ru(II) polypyridyl complexes. (d) Structure of [Os(η^6-biphenyl)$_2$]$^{2+}$ and its [^{1}H,^{187}Os] HMBC spectrum (25 mM in d^4-MeOD at 500 MHz for ^{1}H). Adapted with permission [15]. Copyright © 2009 Wiley-VCH Verlag GmbH & Co. KGaA, Weinheim. (e) Hydrolysis of [(η^5-Cp*)Ir(ppy)Cl] and [(η^5-Cp*)Ir(bpy)Cl]$^+$ under physiological conditions.

Table 2. Examples of recent NMR studies on metal complex–nucleic acid interactions.

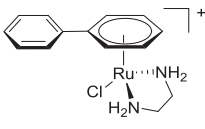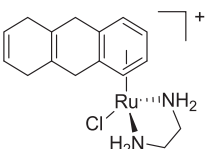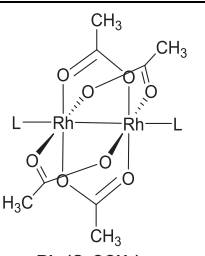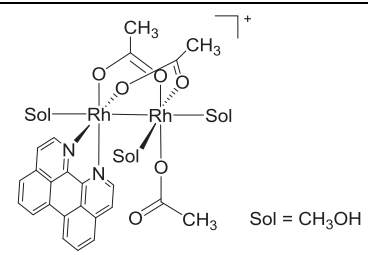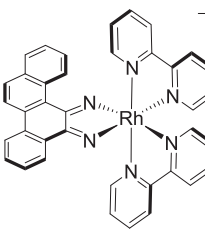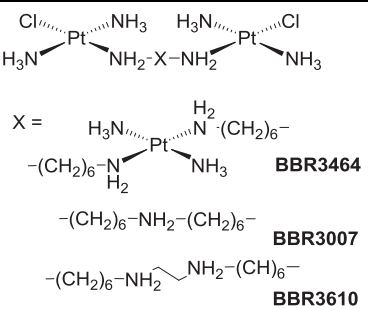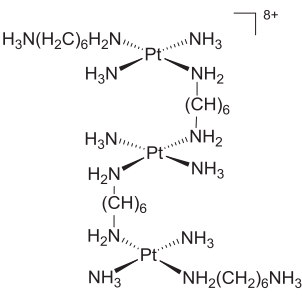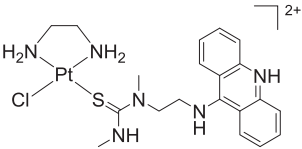| Entry	Compound	DNA oligomers	NMR	Results	Reference
1	 [(η⁶-biphenyl)Ru(en)Cl]⁺	5′-ATACATGGTACATA-3′ 3′-TATGTACCATGTAT-5′	NOESY	Unique binding mode. Ru selective for G N7; uncoordinated phenyl ring intercalates into nearby base pairs.	[9]
2	 [(η⁶-tha)Ru(en)Cl]⁺	5′-CGGCCG-3′ 5′-GCCGGC-3′	[¹H, ¹H] ROESY, NOESY [¹H, ¹⁵N] HSQC [¹H, ³¹P]	Binding mode similar to [(η⁶-biphenyl)Ru(en)Cl]⁺. Binds to G3 and G6 by Ru, intercalation of arene rings.	[10]
3	 Rh₂(O₂CCH₃)₄	5′-CTCTCAACT TCC-3′ 3′-GAGAGTTGAAGG-5′	DQF-COSY NOESY [¹H,¹³C] HSQC	Intrastrand adduct; two Rh centers bind to N4 of C5 and N7 of A6 in major groves. Destabilizes duplex DNA ($\Delta T_m = -22.9\ °C$), weakens base stacking and disrupts H-bonding within the base pairs.	[12]
4	 cis-[Rh₂(dap)(μ-O₂CCH₃)₂(η¹-O₂CCH₃)-(CH₃OH)](O₂CCH₃)]⁺	5′-CCTTCAACTCTC-3′ 3′-GGAAGTTGAGAG-5′	DQF-COSY NOESY	Rh binds to N7 of A6; the planar π-conjugated N^N ligand at the other Rh forms π-stacking interactions with the same A ligand. No significant bending of the aromatic group.	[13]
5	 Δ-[Rh(bpy)₂chrysi]³⁺	5′-CGGA**C**TCCG-3′ 3′-GCCT**C**AGGC-5′	NOESY, COSY, ³¹P NMR	Bulky chrysi ligand selectively inserts into CC mismatched site in minor grove with ejection of mismatched CC to opposite major groove; ³¹P NMR suggests opening of phosphate groups at CC mismatched site to allow space for bulky ligand. No distortion of DNA	[14]
6	 X = BBR3464 BBR3007 BBR3610	5′-ATATGTACATAT-3′ 3′-TATTCATGTATA-5′	[¹H,¹⁵N] HSQC ¹H NMR ³¹P NMR	Kinetics and mechanism; binding of polyamine. Formation of monofunctional adduct with BBR3007 is 3.5-fold faster than BBR3464; BBR3007 and BBR3610 form several conformers with DNA; BBR3464 forms only two conformers.	[23]

Table 2 (*Continued*)

| Entry	Compound	DNA oligomers	NMR	Results	Reference
7	[structure] TriplatinNC(TpNC)	5′-CGCGAATTCGCG-3′ 3′-CGGCTTAAGCGC-5′ 5′-CGTACG-3′ 3′-GCATGC-5′	COSY, TOCSY NOESY HSQC HMQC ^{31}P NMR	Phosphate clamp binding mode: H-bond between ammines on Pt complex and phosphate oxygens. Middle Pt moiety mainly contacts A6, T7 and T8, two terminal Pt moieties interact with C9G10 of both strands.	[24]
8	[structure] [PtCl(en)(ACRAMTU⁻S)]²⁺	5′-CCTCGTCC-3′ 3′-GGAGCAGG-5′	COSY TOCSY NOESY	Dual metallation/intercalation combined 2D NMR and restrained molecular dynamics/molecular mechanics. Pt coordinates to N7 of guanine in major groove; ACRAMTU intercalates into nearby base pairs; duplex DNA stabilized.	[25]

Iridium

Iridium(III) complexes are often considered to be inert in biological systems, but have recently gained increasing attention as anti-cancer agents. Cusanelli *et al.* determined the rate constant for exchange of H_2O on $[Ir(H_2O)_6]^{3+}$ to be 1.1×10^{-10} s^{-1} (~300 years residence time) by ^{17}O NMR [18]. However, if Cp* (η^5-pentamethylcyclopentadienyl anion) is introduced, the hydrolysis (often a key step to activate cytotoxicity in cancer cells) rate is significantly accelerated [19]. For example, the ^{1}H NMR experiments indicate that both [(η^5-Cp*)Ir(bpy)Cl]$^+$ (bpy = 2,2′-biphenyl) and [(η^5-Cp*)Ir(ppy)Cl] (Hppy = 2-phenylpyridine) (Fig. 1E) can undergo rapid hydrolysis (minutes) [20,21]. Surprisingly, the cytotoxicity of [(η^5-Cp*)Ir(ppy)Cl] (IC$_{50}$ = 10.8 μM) is significantly higher than [(η^5-Cp*)Ir(bpy)Cl]$^+$ (IC$_{50}$ > 100 μM). ^{1}H NMR experiments reveal that both complexes form adducts with 9-EtG, but [(η^5-Cp*)Ir(ppy)Cl] also binds to adenine. 2D ^{1}H–^{1}H TOCSY and NOESY NMR further show that the latter complex binds to adenine at N1. The higher lipophilicity (hence higher cellular uptake) and stronger binding with nucleobases may account for the higher cytotoxicity [21]. Notably, the transfer of hydride from NADH to [(η^5-Cp^{xbi-ph})Ir^{III}(ppy)Cl] (Cp^{xbiph} = biphenyltetramethylcyclopentadienyl) to give [(η^5-Cp^{xbiph})Ir^{III}(phpy)(H)] is clear from the high-field-shifted Ir–H ^{1}H NMR peak, δ(^{1}H) = –14.7 ppm [22].

Platinum and gold

Platinum complexes are the most widely investigated metal-based anti-cancer agents. ^{195}Pt (I = 1/2, 33.7% abundance) is useful to study interactions with biomolecules. For example, in the hydrolysis of a Pt(IV) prodrug containing axial haloacetato ligands under physiological conditions, the ^{195}Pt NMR peak for [Pt(dach)(tfa)$_2$(ox)] (dach = cyclohexane-1,2-diamine, tfa = trifluoroacetate, ox = oxalato) shifts from +1625 ppm to +1425 ppm in monohydroxido [Pt(dach)(tfa)(OH)(ox)] and +1310 ppm in dihydroxido [Pt(dach)(OH)$_2$(ox)] (Fig. 2A) [26]. The kinetics of binding of Pt complexes to nucleobases can be determined by ^{195}Pt NMR [27]. Bancroft *et al.* compared the kinetics of reactions of cisplatin and transplatin with DNA. Rate constants for forming monofunctional adducts follow pseudo-first-order kinetics with $k = (10.2 \pm 0.7) \times 10^{-5}$ s^{-1} for cisplatin and $k = (9.6 \pm 0.4) \times 10^{-5}$ for transplatin at pH 6.5 and 37 °C (δ(^{195}Pt) ~ −2300 ppm for both monocomplexes). The rate constant for loss of monofunctional adducts (to form bifunctional adducts) for cisplatin $k = (9.2 \pm 1.4) \times 10^{-5}$ s^{-1} is higher than that for transplatin with $k = (6.3 \pm 0.7) \times 10^{-5}$ s^{-1} [27]. The pK_a values of Pt aqua complexes can be determined by NMR. For example, the pK_a of *trans*-[PtCl(H$_2$O)(^{15}NH$_3$)(c-C$_6$H$_{11}$^{15}NH$_2$)] was determined to be 5.4 by ^{195}Pt NMR, and values for two isomers of *cis*-[PtCl(H$_2$O)(^{15}NH$_3$)(c-C$_6$H$_{11}$^{15}NH$_2$)] were the same (6.73) by [^{1}H,^{15}N] HSQC NMR [28].

For cisplatin and its derivatives, the *trans*-influence of L in ^{15}N–^{195}Pt–L strongly influences both the ^{15}N chemical shift and ^{195}Pt–^{15}N coupling constant (^1J(^{195}Pt–^{15}N; see Fig. 2B) [29–31]. For example, the binding of *cis*-[PtCl$_2$(^{15}NH$_3$)$_2$] to the protein kinase Mnk1 or *apo*Mnk1 leads to a significant change in ^{15}N shift. As shown in the [^{1}H,^{15}N] HSQC NMR spectra (Fig. 2C, a–c), δ(^{15}N) of ^{15}N-labeled cisplatin at −67 ppm shifts to −66 and −83 ppm for the mono-aqua species [32]. After 3-hours incubation with *apo*Mnk1, new peaks with δ(^{15}N) of −66 and −38 ppm appeared, corresponding to *cis*-[PtCl(^{15}NH$_3$)$_2$S$_{cys}$] species. Further incubation for
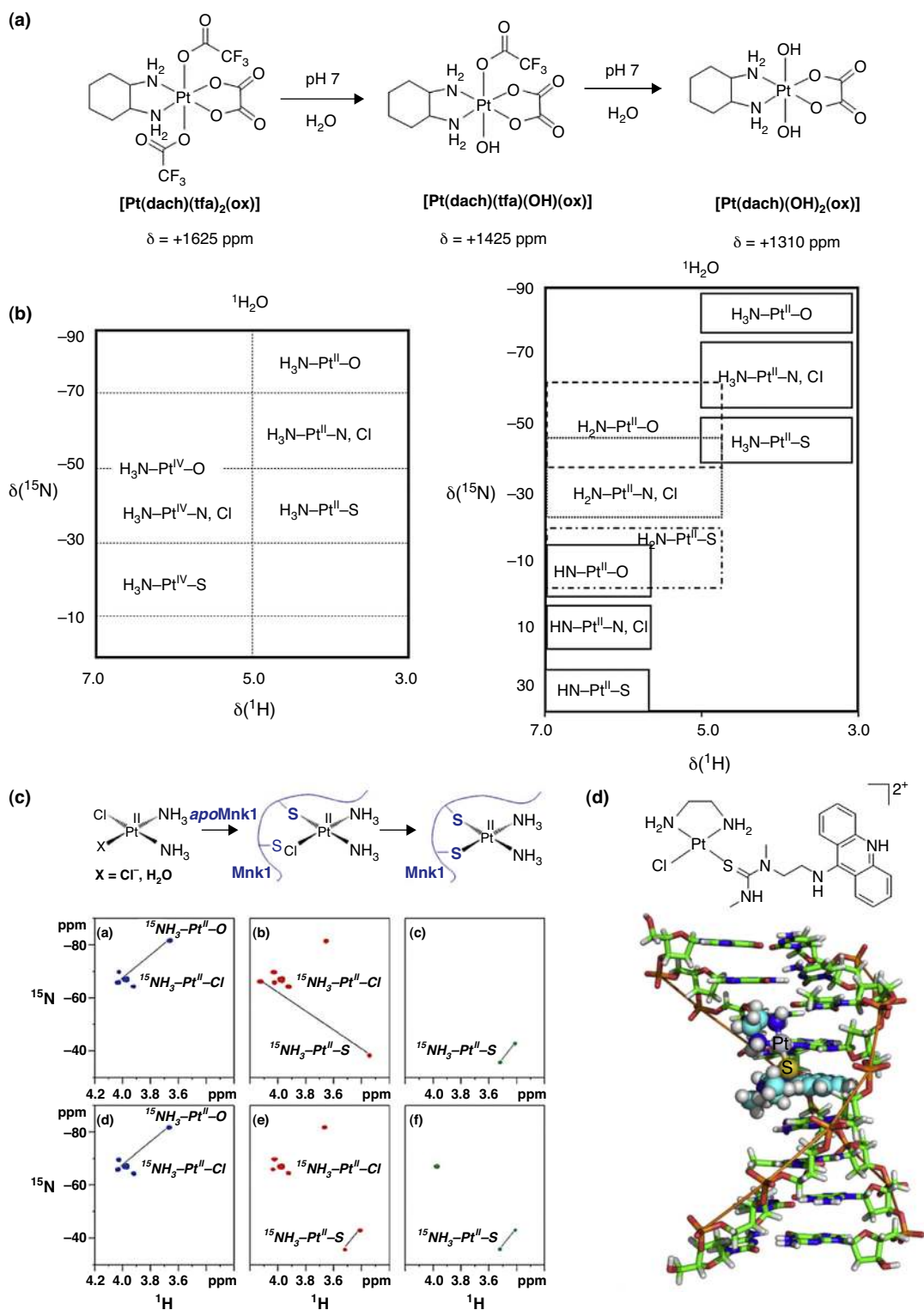
Figure 2. (a) Hydrolysis of Pt(IV) complex [Pt(dach)(tfa)$_2$(ox)]. (b) Left: range of $\delta(^1H)$ and $\delta(^{15}N)$ in NH$_3$–Pt^{II} and NH$_3$–Pt^{IV} with different *trans*-ligands. Right: range of $\delta(^1H)$ and $\delta(^{15}N)$ in NH$_3$–Pt^{II}, NH$_2$–Pt^{II}, NH–Pt^{II} with different *trans*-ligands. Adapted with permission [31]. Copyright © 1996 Published by Elsevier B.V. (c) Binding of *cis*-[(PtCl)$_2$](^{15}NH$_3$)$_2$ to protein kinase. [^{1}H,^{15}N] HSQC spectra of *cis*-PtCl$_2$(^{15}NH$_3$)$_2$ mixed with equimolar ratio of (a–c) apoMnk1 and (d–f) Cu$^+$–Mnk1 at 0 hours (a and d), 3 hours (b and e), and 24 hours (c and f). Reproduced with permission [32]. Copyright © 2014 Wiley-VCH Verlag GmbH & Co. KGaA, Weinheim. (d) 3D structure of [PtCl(en)(ACRAMTU-S)]$^{2+}$ binding to DNA oligonucleotide. Redrawn from PDB 1XRW [25].

24 hours resulted in $\delta(^{15}N)$ at -43 and -36 ppm attributable to $\{Pt(^{15}NH_3)_2\}$ binding to two cysteine residues. The $[^1H,^{15}N]$ HSQC NMR experiments with Cu^+-Mnk1 similarly show the binding of cis-$\{Pt(^{15}NH_3)_2\}$ species to cysteine residues of the protein, suggestive of replacement of Cu^+ by cis-$\{Pt(^{15}NH_3)_2\}^{2+}$ (Fig. 2C, d–f). Such results were confirmed by $[^1H,^{13}C]$ HSQC experiments for the mixture of $^{15}N,^{13}C$-Cys labeled kinase with cisplatin [32]. A similar interaction was identified by $[^1H,^{15}N]$ HSQC NMR for cisplatin with ^{15}N-labeled Cu chaperone Atox1 [33]. Besides binding to cysteine thiols, Pt drugs can also bind to methionine sulfur (leading to a S chiral center) before reaching their DNA target. The binding of $[Pt(dien)Cl]^+$ (dien = diethylenetriamine) to Met studied by $[^1H,^{15}N]$ HSQC NMR showed an interchange between S- and N-bound Met. Lowing the pH to 3 resulted in the ring-opened product $[Pt(dienH-N,N')(L-Met-S,N)]$, where the existence of two chiral centers at S and $C\alpha$ of Met gives rise to four diastereomers [34].

$[^1H,^{15}N]$ 2D HSQC NMR is useful in the study of non-covalent binding. Ruhayel et al. investigated polyamine-DNA interactions through $[^1H,^{15}N]$ 2D HSQC NMR (Table 2, entry 6) [23]. The replacement of the central Pt-tetraam(m)ine unit in $[\{trans-PtCl(NH_3)_2\}_2(\mu-trans-Pt-(NH_3)_2\{NH_2(CH_2)_6NH_2\}_2)]^{4+}$ (BBR3464) by an amine (BBR3007) or ethylendiamine (BBR3610) unit shows several binding conformers while BBR3464 only has two discrete conformers, which is a possible reason for the more potent cytotoxicity of the latter two complexes than BBR3464. Qu et al. studied phosphate clamp binding of TriplatinNC to a DNA oligonucleotide (Table 2, entry 7) [24]. Significant changes in $^1H,^{15}N$ chemical shifts and $^1J(^{195}Pt-^{15}N)$ couplings indicated formation of H-bonds between ammine of Pt complexes and phosphate oxygens.

The 3D NMR structure of $[PtCl(en)(ACRAMTU-S)]^{2+}$ (ACRAMTU = 1-[2-(acridin-9-ylamino)ethyl]-1,3-dimethylthiourea) bound to a DNA oligonucleotide (together with restrained molecular dynamics/molecular mechanics) indicates a dual metalation of N7 of guanine and an intercalation of the acridine moiety into neighboring base pairs (Table 2, entry 6 and Fig. 2D) [25]. Multinuclear NMR experiments on the photo-induced Pt(IV) to Pt(II) activation of cis,trans,cis-$[Pt^{IV}(N_3)_2(OH)_2(NH_3)_2]$ in the presence of 1-methylimidazole (1-MeIm) showed photo-isomerization and trans-labilisation products, accompanied by release of N_3^-, ammonia, and formation of O_2 under 365 nm UVA irradiation [35].

Owing to the extremely low magnetogyric ratio and large quadruple moment of ^{197}Au, NMR studies on gold complexes are focused only on ligand nuclei. Ligand exchange reactions of $[Au^I(NHC)_2]^+$ (NHC = N-heterocyclic carbene) with cysteine/selenocysteine [36], Au(III) reduction to Au(I) [37], and binding interactions of gold(I) complexes with model peptides [38] have been investigated by ^1H NMR.

Other NMR methods

NMR can be applied to more complicated systems such as biofluids, including use of high resolution magic angle spinning (HR-MAS) to sharpen broad peaks and study metabolite profiling [39], and drug delivery systems [40]. HR-MAS is commonly used in solid state NMR (ssNMR) to study polymers, nanoparticles and supramolecular systems [41]. Notably, paramagnetic effects can be useful and have practical applications. Paramagnetic gadolinium-based magnetic resonance imaging (MRI) contrast agents have been widely used for body imaging by shortening the relaxation times of ^1H in H_2O which interacts with contrast agents. NMR can be coupled with HPLC and mass spectrometry; the combined HPLC-^1H NMR-MS detection is a powerful method to study complicated mixtures of for example, metabolites in human urine, by continuous flow [42].

Conclusion

NMR spectroscopy is making important contributions to understanding the molecular mechanisms of action of anti-cancer metal complexes by providing valuable insights into their chemical speciation in biological systems. The sensitivity of nuclei to detection is a key concern for NMR characterization and currently most NMR studies are based on ligand rather than metal nuclei. The sensitivity of metal nuclei (as well as other heteronuclei) can often be enhanced by isotope enrichment and polarization transfer methods. Representative examples of NMR studies on precious metal complexes interacting with biomolecules (e.g., DNA, proteins) highlight the powerful potential of NMR spectroscopy for studying, not only the structures, but also the thermodynamics and kinetics of chemical speciation of therapeutic metal complexes in biological systems.

Conflict of interest

The authors declare no conflicts of interest.

Acknowledgements

References

[1] Barry NPE, Sadler PJ. Exploration of the medical periodic table: towards new targets. Chem Commun 2013;49:5106–31.

[2] Zou T, Lum CT, Lok C-N, Zhang J-J, Che C-M. Chemical biology of anticancer gold(III) and gold(I) complexes. Chem Soc Rev 2015. http://dx.doi.org/10.1039/C1035CS00132C. Advance Article.

[3] Ronconi L, Sadler PJ. Applications of heteronuclear NMR spectroscopy in biological and medicinal inorganic chemistry. Coord Chem Rev 2008;252:2239–77.

[4] Lee JH, Okuno Y, Cavagnero S. Sensitivity enhancement in solution NMR: emerging ideas and new frontiers. J Magn Reson 2014;241:18–31.

[5] Morris GA, Freeman R. Enhancement of nuclear magnetic resonance signals by polarization transfer. J Am Chem Soc 1979;101:760–2.

[6] Ni Dhubhghaill OM, Hagen WR, Keppler BK, Lipponer K-G, Sadler PJ. Aquation of the anticancer complex trans-[RuCl$_4$(Him)$_2$]$^-$ (Him = imidazole). J Chem Soc Dalton Trans 1994;3305–10.

[7] Chen Y, Lin F-T, Shepherd RE. ^{15}N NMR and electrochemical studies of [Ru^{II}(hedta)]$^-$ complexes of NO, NO$^+$, NO$_2^-$, and NO$^-$. Inorg Chem 1999;38:973–83.

[8] Xie X, Mulcahy SP, Meggers E. Strategy for the stereochemical assignment of tris-heteroleptic Ru(II) complexes by NMR spectroscopy. Inorg Chem 2009;48:1053–61.

[9] Liu H-K, Berners-Price SJ, Wang F, Parkinson JA, Xu J, Bella J, et al. Diversity in guanine-selective DNA binding modes for an organometallic ruthenium arene complex. Angew Chem Int Ed 2006;45:8153–6.

[10] Liu H-K, Parkinson JA, Bella J, Wang F, Sadler PJ. Penetrative DNA intercalation and G-base selectivity of an organometallic tetrahydroanthracene Ru^{II} anticancer complex. Chem Sci 2010;1:258–70.

[11] Elsevier CJ, Kowall B, Kragten H. Steric and electronic effects on the ^{103}Rh NMR shifts of (COD)Rh(phosphine) complexes. Inorg Chem 1995;34:4836–9.

[12] Kang M, Chifotides HT, Dunbar KR. 2D NMR study of the DNA duplex d(CTCTC*A*ACTTCC)·d(GGAAGTTGAGAG) cross-linked by the antitumor-active dirhodium(II,II) unit at the cytosine–adenine step. Biochemistry 2008;47:2265–76.

[13] Kang M, Chouai A, Chifotides HT, Dunbar KR. 2D NMR spectroscopic evidence for unprecedented interactions of cis-[Rh$_2$(dap)(μ-O$_2$CCH$_3$)$_2$(η^1-O$_2$CCH$_3$)(CH$_3$OH)](O$_2$CCH$_3$) with a DNA oligonucleotide: combination of intercalative and coordinative binding. Angew Chem Int Ed 2006;45:6148–51.

[14] Cordier C, Pierre VC, Barton JK. Insertion of a bulky rhodium complex into a DNA cytosine–cytosine mismatch: an NMR solution study. J Am Chem Soc 2007;129:12287–95.

[15] Bell AG, Koźmiński W, Linden A, von Philipsborn W. ^{187}Os NMR study of (η^6-arene)osmium(II) complexes: separation of electronic and steric ligand effects. Organometallics 1996;15:3124–35.

[16] Gray JC, Pagelot A, Collins A, Fabbiani FPA, Parsons S, Sadler PJ. Organometallic osmium(II) and ruthenium(II) biphenyl sandwich complexes: X-ray crystal structures and 187Os NMR spectroscopic studies in solution. Eur J Inorg Chem 2009;2009:2673–7.

[17] Fu Y, Romero MJ, Habtemariam A, Snowden ME, Song L, Clarkson GJ, et al. The contrasting chemical reactivity of potent isoelectronic iminopyridine and azopyridine osmium(ii) arene anticancer complexes. Chem Sci 2012;3:2485–94.

[18] Cusanelli A, Frey U, Richens DT, Merbach AE. The slowest water exchange at a homoleptic mononuclear metal center: variable-temperature and variable-pressure ^{17}O NMR study on [Ir(H$_2$O)$_6$]$^{3+}$. J Am Chem Soc 1996;118:5265–71.

[19] Liu Z, Sadler PJ. Organoiridium complexes: anticancer agents and catalysts. Acc Chem Res 2014;47:1174–85.

[20] Liu Z, Habtemariam A, Pizarro AM, Fletcher SA, Kisova A, Vrana O, et al. Organometallic half-sandwich iridium anticancer complexes. J Med Chem 2011;54:3011–26.

[21] Liu Z, Salassa L, Habtemariam A, Pizarro AM, Clarkson GJ, Sadler PJ. Contrasting reactivity and cancer cell cytotoxicity of isoelectronic organometallic iridium(III) complexes. Inorg Chem 2011;50:5777–83.

[22] Liu Z, Romero-Canelón I, Qamar B, Hearn JM, Habtemariam A, Barry NPE, et al. The potent oxidant anticancer activity of organoiridium catalysts. Angew Chem Int Ed 2014;53:3941–6.

[23] Ruhayel RA, Langner JS, Oke MJ, Berners-Price SJ, Zgani I, Farrell NP. Chimeric platinum-polyamines and DNA binding kinetics of DNA interstrand cross-link formation by dinuclear platinum complexes with polyamine linkers. J Am Chem Soc 2012;134:7135–46.

[24] Qu Y, Kipping RG, Farrell NP. Solution studies on DNA interactions of substitution-inert platinum complexes mediated via the phosphate clamp. Dalton Trans 2015;44:3563–72.

[25] Baruah H, Wright MW, Bierbach U. Solution structural study of a DNA duplex containing the guanine-N7 adduct formed by a cytotoxic platinum-acridine hybrid agent. Biochemistry 2005;44:6059–70.

[26] Wexselblatt E, Yavin E, Gibson D. Platinum(IV) prodrugs with haloacetato ligands in the axial positions can undergo hydrolysis under biologically relevant conditions. Angew Chem Int Ed 2013;52:6059–62.

[27] Bancroft DP, Lepre CA, Lippard SJ. ^{195}Pt NMR kinetic and mechanistic studies of cis- and trans-diamminedichloroplatinum(II) binding to DNA. J Am Chem Soc 1990;112:6860–71.

[28] Barton SJ, Barnham KJ, Habtemariam A, Sue RE, Sadler PJ. pK_a values of aqua ligands of platinum(II) anticancer complexes: [^{1}H,^{15}N] and ^{195}Pt NMR studies of cis- and trans-[PtCl$_2$(NH$_3$)(cyclohexylamine)]. Inorg Chim Acta 1998;273:8–13.

[29] Kerrison SJS, Sadler PJ. The trans influence in platinum chemistry. A platinum-195 nuclear magnetic resonance study of [^{15}N]nitrito-, chloro-, and bromo-platinum-(II) and -(IV) complexes. J Chem Soc Dalton Trans 1982;2363–9.

[30] Motschi H, Nussbaumer C, Pregosin PS, Bachechi F, Mura P, Zambonelli L. The trans-influence in platinum(II) complexes ^{1}H- and ^{13}C-NMR. and X-ray structural studies of tridentate Schiff's base complexes of platinum (II). Helv Chim Acta 1980;63:2071–86.

[31] Berners-Price SJ, Ronconi L, Sadler PJ. Insights into the mechanism of action of platinum anticancer drugs from multinuclear NMR spectroscopy. Prog Nucl Magn Reson Spectrosc 2006;49:65–98.

[32] Tadini-Buoninsegni F, Bartolommei G, Moncelli MR, Inesi G, Galliani A, Sinisi M, et al. Translocation of platinum anticancer drugs by human copper ATPases ATP7A and ATP7B. Angew Chem Int Ed 2014;53:1297–301.

[33] Palm ME, Weise CF, Lundin C, Wingsle G, Nygren Y, Björn E, et al. Cisplatin binds human copper chaperone Atox1 and promotes unfolding in vitro. Proc Natl Acad Sci 2011;108:6951–6.

[34] Chen Y, Guo Z, del Socorro Murdoch P, Zang E, Sadler PJ. Interconversion between S- and N-bound L-methionine adducts of Pt(dien)$^{2+}$ (dien = diethylenetriamine) via dien ring-opened intermediates. J Chem Soc Dalton Trans 1998;1503–8.

[35] Phillips HIA, Ronconi L, Sadler PJ. Photoinduced reactions of cis,trans,cis-[Pt^{IV}(N$_3$)$_2$(OH)$_2$(NH$_3$)$_2$] with 1-methylimidazole. Chem Eur J 2009;15:1588–96.

[36] Hickey JL, Ruhayel RA, Barnard PJ, Baker MV, Berners-Price SJ, Filipovska A. Mitochondria-targeted chemotherapeutics: the rational design of gold(I) N-heterocyclic carbene complexes that are selectively toxic to cancer cells and target protein selenols in preference to thiols. J Am Chem Soc 2008;130:12570–71.

[37] Zou T, Lum CT, Chui SS-Y, Che C-M. Gold(III) complexes containing N-heterocyclic carbene ligands: thiol 'switch-on' fluorescent probes and anti-cancer agents. Angew Chem Int Ed 2013;52:2930–3.

[38] Zou T, Lum CT, Lok C-N, To W-P, Low K-H, Che C-M. A binuclear gold(I) complex with mixed bridging diphosphine and bis(N-heterocyclic carbene) ligands shows favorable thiol reactivity and inhibits tumor growth and angiogenesis in vivo. Angew Chem Int Ed 2014;53:5810–4.

[39] Saric J, Li JV, Wang Y, Keiser J, Veselkov K, Dirnhofer S, et al. Panorganismal metabolic response modeling of an experimental echinostoma caproni infection in the mouse. J Proteome Res 2009;8:3899–911.

[40] Mantle MD. NMR and MRI studies of drug delivery systems. Curr Opin Colloid Interface Sci 2013;18:214–27.

[41] Chierotti MR, Gobetto R. Solid-state NMR studies on supramolecular chemistry. In: Supramol. Chem.. John Wiley & Sons, Ltd.; 2012.

[42] Shockcor JP, Unger SE, Wilson ID, Foxall PJD, Nicholson JK, Lindon JC. Combined HPLC NMR spectroscopy, and ion-trap mass spectrometry with application to the detection and characterization of xenobiotic and endogenous metabolites in human urine. Anal Chem 1996;68:4431–5.